View metadata, citation and similar papers at core.ac.uk

brought to you by CORE

provided by Nottingham ePrints

Zhang, Bo and Abu-Khumra, Sabah and Aibout, Abdellah and Horsewill, Anthony J. (2017) Manipulating and probing the polarisation of a methyl tunnelling system by field-cycling NMR. Journal of Chemical Physics, 146 (6). 064302. ISSN 1089-7690

Access from the University of Nottingham repository:
http://eprints.nottingham.ac.uk/41117/1/pdf_archiveJCPSA6vol_146iss_6064302_1_am.pdf

Copyright and reuse:

The Nottingham ePrints service makes this work by researchers of the University of Nottingham available open access under the following conditions.

This article is made available under the University of Nottingham End User licence and may be reused according to the conditions of the licence. For more details see: http://eprints.nottingham.ac.uk/end_user_agreement.pdf

A note on versions:

The version presented here may differ from the published version or from the version of record. If you wish to cite this item you are advised to consult the publisher's version. Please see the repository url above for details on accessing the published version and note that access may require a subscription.

For more information, please contact eprints@nottingham.ac.uk

AIP Publishing

This manuscript was accepted by J. Chem. Phys. Click here to see the version of record.

Manipulating and probing the polarisation of a methyl tunnelling system by field-cycling NMR

Bo Zhang[1,2], Sabah M.M. Abu-Khumra[1$], Abdellah Aibout[3#] & Anthony J Horsewill[1*]

[1] *School of Physics & Astronomy, University of Nottingham, Nottingham, NG7 2RD, UK*

[2] *CAS Key Laboratory of Microscale Magnetic Resonance and Department of Modern Physics, University of Science and Technology of China, Hefei 230026, China*

[3] *Laboratoire de Spectroscopie des Materiaux, Université de Mostaganem, B.P. 227, Mostaganem 2700, Algeria*

[*]Corresponding author: a.horsewill@nottingham.ac.uk

Abstract

In NMR the polarisation of the Zeeman system may be routinely probed and manipulated by applying resonant rf pulses. As with spin-½ nuclei, at low temperature the quantum tunnelling states of a methyl rotor are characterised by two energy levels and it is interesting to consider how these tunnelling states might be probed and manipulated in an analogous way to nuclear spins in NMR. In this paper experimental procedures based on magnetic field-cycling NMR are described where, by irradiating methyl tunnelling sidebands, the polarisations of the methyl tunnelling systems are measured and manipulated in a prescribed fashion. At the heart of the technique is a phenomenon that is closely analogous to dynamic nuclear polarisation and the solid effect where forbidden transitions mediate polarisation transfer between ^{1}H Zeeman and methyl tunnelling systems. Depending on the irradiated sideband, both positive and negative polarisations of the tunnelling system are achieved, the latter corresponding to population inversion and negative tunnelling temperatures. The transition mechanics are investigated through a series of experiments and a theoretical model is presented that provides good quantitative agreement.

[#] Now at: Laboratoire L.E.O.G, Ecole Normale Supérieure, B.P. 227, Mostaganem 27000, Algeria

[$] Now at: Department of Laser Physics, College of Science for Women, University of Babylon, Ministry of Higher Education and Scientific Research, Hilla, P.O.00964, Iraq

ACCEPTED MANUSCRIPT

AIP Publishing

This manuscript was accepted by J. Chem. Phys. Click here to see the version of record.

1. Introduction

Interesting quantum effects that have no classical analogue arise when spatial and nuclear spin degrees of freedom are combined in the description of symmetrical quantum rotors. At their heart is the antisymmetry principle which underpins the Pauli Exclusion Principle (PEP), requiring the complete wavefunction describing the rotor to be antisymmetric upon exchange of indistinguishable fermions. The wavelike characteristics of the rotor are naturally evident in the quantisation of energy and angular momentum, however, the PEP additionally leads to a partitioning of the eigenstates into discrete sets of nuclear spin isomers, alternatively described as nuclear spin-symmetry species. The most familiar example is molecular hydrogen which is characterised by two spin-isomers, *ortho*-H_2 and *para*-H_2. The discrete combination of spatial and nuclear spin states is evident in that *ortho*-H_2 has total nuclear spin $I=1$ and odd values of the rotational quantum number $J=1,3,\ldots$, whereas *para*-H_2 has $I=0$ and even values of J. Particularly at low temperature, the two sets of nuclear spin isomers often co-exist as independent species, remaining decoupled from each other for substantial periods of time. This is evident for the endofullerene $H_2@C_{60}$ [1-3] where, in the absence of spin conversion catalysts, interconversion between *ortho*- and *para*-hydrogen cannot be detected in experiments conducted over several days. Analogous behaviour can be observed even for molecules which have a lower degree of symmetry, as exemplified by the long-lived singlet states identified by the group of Levitt. [4-6]

Methyl groups, CH_3, are quantum rotors with a three-fold symmetry axis. Rotation about the C_3 axis permutes the indistinguishable ^1H nuclei belonging to the three hydrogen atoms. As a result we identify two discrete sets of spin-symmetry species labelled A and E, classified by the irreducible representations of the C_3 symmetry group [7, 8]. The A-species is a quartet with total nuclear spin $I=3/2$ whereas there are two degenerate E-species, labelled E_a and E_b, which both have spin $I=1/2$. In a molecular environment there is a potential barrier to rotation and coherent quantum tunnelling gives rise to a splitting of the A- and E-species which are separated in energy by $h\nu_t$, where ν_t is the tunnelling frequency.

In accordance with the PEP, the spin-symmetry species of CH_3 are characterised by certain allowable combinations of space and spin wave-functions [9]. Transitions between A and E species involve simultaneous changes in spatial and spin eigenstates. As a result, at low temperature the interconversion is spin-restricted and relatively slow so we can identify a long-lived 'tunnelling reservoir' characterised by the energy $h\nu_t$ and the polarisation of the A- and E-states. To investigate the tunnelling dynamics demands an

ACCEPTED MANUSCRIPT

AIP Publishing

This manuscript was accepted by J. Chem. Phys. Click here to see the version of record.

interaction that has the capacity to bring about simultaneous changes in space and spin states and hence induce transitions between A- and E-species. One such interaction is the ^{1}H-^{1}H dipole-dipole interaction, which has played an important role in elucidating the quantum dynamics of this quantum rotor [8, 10].

Having discrete combinations of space and nuclear spin eigenfunctions, spin-isomers offer opportunities to act as vehicles for creating strongly non-equilibrium nuclear spin polarisations. This is well-established in the technique of PHIP (parahydrogen induced polarisation) and related techniques where *para*-H_2 is used as a hyperpolarisation agent [11]. It may be envisaged that given appropriately designed experimental protocols, the spin-symmetry species characterising other quantum rotors may be analogously exploited. In this respect, methyl groups have a potential advantage over molecular hydrogen because the splitting between states of different spin-symmetry is a variable of the height and shape of a potential barrier, and hence determined by the local molecular environment. Therefore, the A-E energy splitting may be optimally 'selected' by appropriate choice of host molecule. Indeed, progress has been made in utilising the Haupt effect, a phenomenon that applies to weakly hindered CH_3 groups [12, 13], in nuclear polarisation schemes. Additionally, the group of Levitt has explained and exploited remarkable hyperpolarisation effects in solution NMR attributed to quantum rotor effects of CH_3 [5, 14, 15] which were first observed by Icker and Berger [16, 17].

To create non-equilibrium spin polarisation in methyl group containing materials, the protocols demand A-E transitions to be driven directly. Therefore, it is interesting to explore mechanisms and experimental protocols that will enable the polarisation of the tunnelling reservoir to be manipulated by design, somewhat analogous to the ubiquitous manipulation of spin states using pulsed NMR. This is the motivation for this paper. Although the polarisations achieved here are relatively modest, largely because the tunnelling frequencies are relatively small, field-cycling NMR sequences have been devised to purposely drive positive and negative changes in both tunnelling and ^{1}H-polarisations, allowing an exploration of the fundamental principles that may later be developed to form the foundations of protocols achieving more substantial spin polarisations.

In an earlier paper [18], we described experiments that enabled the polarisation of the tunnelling reservoir to be manipulated and interrogated directly. These experiments demanded rf irradiation at low magnetic field and excursions to level-(anti)crossings that arise between A and E states at particular magnetic fields. Therefore, magnetic field-cycling was incorporated in the NMR pulse sequence and the phenomenon was described as *Dynamic Tunnelling Polarisation* (DTP) because of its close analogy to dynamic nuclear polarisation (DNP) and the solid effect [18-20]. In this new study, DTP experiments

ACCEPTED MANUSCRIPT

AIP Publishing

This manuscript was accepted by J. Chem. Phys. Click here to see the version of record.

on acetophenone, 2-butanone and thioanisole are described. These materials are characterised by tunnelling frequencies in the range 490 kHz – 1.5 MHz. Field-cycling NMR experiments have been employed to quantify the positive and negative changes in ^{1}H polarisation that come about when 'tunnelling sidebands' are irradiated using rf. The mechanisms are investigated, including the measurement of the lifetime of the tunnelling reservoir and the role of the level-crossings in inducing resonant A-E conversion. Finally, the experimental results are successfully simulated using a thermodynamic model.

2. Theoretical background

In a condensed phase, CH_3 rotors are sub-groups of a molecule, with the result that inter- and intra-molecular interactions give rise to a potential barrier to rotation about the three-fold axis. This barrier has 3-fold symmetry (or higher harmonics) and rotation of the molecule permutes the hydrogen atoms between energetically equivalent sites. Quantum mechanically, exchange interactions associated with tunnelling through the potential barrier give rise to a splitting of the ground torsional state and A- and E-species are separated in energy by $h\nu_t$, where the tunnelling frequency ν_t is an exponential function of the barrier properties[21].

The NMR properties of the methyl rotor may be described by the spin Hamiltonian [10],

$$\hat{H}_s = \hat{H}_Z + \hat{H}_t + \hat{H}_{dd} \qquad (1)$$

where $\hat{H}_Z = -\hbar\gamma B_z \sum_{j=1}^{3} \hat{I}_{jz}$ is the Zeeman interaction of the three ^{1}H spins labelled $j = 1,2,3$ with the applied field B_z oriented along the z-axis. $\hat{H}_{dd}$ is the ^{1}H-^{1}H dipole-dipole interaction and $\hat{H}_t$ is an equivalent exchange operator that incorporates the tunnelling splitting into a spin Hamiltonian formalism. Following Apaydin and Clough [10] we may write,

$$\hat{H}_t = -\tfrac{2}{3} h\nu_t \sum_{j>k} \hat{\mathbf{I}}_j . \hat{\mathbf{I}}_k \qquad (2)$$

The dipolar interaction is between the three pairs of ^{1}H spins comprising the CH_3 rotor,

$$\hat{H}_{dd} = \sum_{j>k} \sum_{q=-2}^{2} F_{jk}^{(q)} \hat{A}_{jk}^{(q)} \qquad (3)$$

which has the important association of a spatial factor $F_{jk}^{(q)}$ with a factor $\hat{A}_{jk}^{(q)}$ comprising nuclear spin operators characterised by $q = 0, \pm 1, \pm 2$ spin flip terms. In coupling space

ACCEPTED MANUSCRIPT

AIP Publishing

This manuscript was accepted by J. Chem. Phys. Click here to see the version of record.

and spin, $\hat{H}_{dd}$ is significant to quantum rotor physics, providing a conduit for interactions between A and E spin-symmetry species. Explicit expressions for $F_{jk}^{(q)}$ and $\hat{A}_{jk}^{(q)}$ are available in the NMR literature and have been defined in the context of methyl rotors in reference [22], showing how $\hat{H}_{dd}$ may be written in symmetry-adapted form, explicitly revealing its capacity to drive A-E transitions.

Solving the spin Hamiltonian Eq.(1) in a basis of nuclear spin eigenfunctions $\left|m_I^{(1)}m_I^{(2)}m_I^{(3)}\right\rangle$ provides the manifold of tunnelling-Zeeman eigenstates that characterise the CH_3 rotor ($m_I=\pm\frac{1}{2}$). There are six non-degenerate energy levels and plotting the magnetic field dependence reveals the presence of two sets of level-(anti)crossings; lc1 where the ^{1}H Zeeman frequency ν_H equals the tunnelling frequency, ($\nu_H=\gamma B_z/2\pi=\nu_t$) and lc2 where $\nu_H=\nu_t/2$; see Fig. 1a. Within the manifold of levels we identify pure Zeeman transitions with frequencies ν_H and $2\nu_H$ and tunnelling sideband transitions with frequencies $\nu_H\pm\nu_t$ and $2\nu_H\pm\nu_t$.

The A and E species are only weakly coupled so we identify the tunnelling reservoir characterised by energy $h\nu_t$ and polarisation $P_{tun}=\left(p_A-p_E\right)/\left(p_A+p_E\right)$. The Boltzmann populations $p_{A,E}$ of the two species also define the inverse tunnelling temperature, β_t. The latter may remain out of equilibrium with the inverse lattice temperature for substantial periods of time due to the long lifetimes of the A and E states.

The spin-lattice relaxation time, T_1, is also long at low temperature and we similarly identify the ^{1}H Zeeman reservoir characterised by energy $h\nu_H$ and ^{1}H spin polarisation $P_Z=\left(p_+-p_-\right)/\left(p_++p_-\right)$, where $p_{+,-}$ are the Boltzmann populations of the $m_I=\pm\frac{1}{2}$ states of ^{1}H. In turn these populations also define the inverse Zeeman temperature, β_Z.

Ignoring small dipolar shifts the energy levels of the tunnelling-Zeeman manifold approximate to,

$$E_i=h\nu_H m_i+h\nu_t n_i \qquad (4)$$

where $m_i=\frac{3}{2},\frac{1}{2},-\frac{1}{2},-\frac{3}{2}$ and $n_i=-\frac{1}{2}$ are magnetic and tunnelling quantum numbers respectively for A-species, and $m_i=\frac{1}{2},-\frac{1}{2}$ and $n_i=+\frac{1}{2}$ for E-species. This provides an equivalent formalism for defining the thermodynamic properties of the tunnelling-

ACCEPTED MANUSCRIPT

AIP Publishing

This manuscript was accepted by J. Chem. Phys. Click here to see the version of record.

Zeeman system. In the high temperature approximation we may define the populations of the tunnelling-Zeeman levels as ,

$$p_i = \beta_Z m_i \nu_H + \beta_t n_i \nu_t \qquad (5)$$

where any constants have been ignored since only population differences are important. In this way the populations can be defined in terms of the inverse tunnelling and Zeeman temperatures. Alternatively, the inverse temperatures can be defined in terms of the populations using,

$$\beta_Z = \sum_i p_i m_i \Big/ \nu_H \sum_i m_i^2 \quad \text{and} \quad \beta_t = \sum_i p_i n_i \Big/ \nu_t \sum_i n_i^2 \qquad (6)$$

Given $P_Z \propto B_z \beta_Z$ and $P_t \propto \beta_t$, Eqs. (4)-(6) will later provide a theoretical framework for numerical simulations of the experiments conducted in this investigation.

3. Experimental details

Experiments were conducted using the Nottingham field-cycling NMR spectrometer, described elsewhere . The NMR pulse sequences employed in this investigation are illustrated in Fig. 2. Both sequences begin with a saturation train of $\frac{\pi}{2}$-pulses on resonance with the ^{1}H spins at the field $B_{nmr} \approx 0.86$ T. The spins are then polarised at the field B_{pol} for time τ_{pol} before switching the field rapidly ($3 \leq \Delta B/\Delta t \leq 10$ T s^{-1}) to low field B_{lf} . Here the sample is irradiated with rf at frequency ν_{rf} for time τ_{lf} . The interest is in the changes that the rf irradiation induces in the thermodynamic states of the Zeeman and tunnelling reservoirs. The Zeeman state can be interrogated by a $\frac{\pi}{2}$-pulse, however to identify the influence on the tunnelling state a more indirect method is required. In Fig. 2a, the field is first switched rapidly to NMR resonance where the ^{1}H spins are saturated with a burst of resonant pulses, rendering the ^{1}H spin polarisation $P_Z = 0$. Meanwhile, at that high field B_{nmr} , the rf pulses have no influence on the tunnelling state. Subsequently, by switching the field to a level-crossing, lc1 or lc2, the tunnelling and Zeeman systems will rapidly equilibrate and any tunnelling polarisation will be transferred to the previously saturated ^{1}H Zeeman reservoir. In the pulse sequence, Fig. 2a, this field is labelled B_{LC}. Finally, a $\frac{\pi}{2}$-pulse at the field B_{nmr} enables that ^{1}H spin polarisation to be measured, from which we can infer the tunnelling polarisation that existed at the end of the rf irradiation.

The variant of the field-cycling pulse sequence, Fig. 2b, contains an additional 'relaxation' step, inserted immediately after the rf irradiation. During this period the

ACCEPTED MANUSCRIPT

AIP Publishing

This manuscript was accepted by J. Chem. Phys. Click here to see the version of record.

tunnelling reservoir may relax towards equilibrium with the lattice and by plotting the final tunnelling polarisation as a function of τ_{rel}, the tunnelling relaxation time may be determined. The field at which the relaxation is conducted, B_{rel}, is a variable of the experiment enabling the relaxation to be investigated close by or remote from the level crossing fields.

All experiments were conducted with a sample temperature of 4.2 K. The samples of thioanisole ($C_6H_5SCH_3$), acetophenone ($C_6H_5C(O)CH_3$) and 2-butanone ($CH_3C(O)CH_2CH_3$) were obtained from Aldrich and used as supplied. All three are liquids at room temperature. Quench cooling invariably rendered a solid sample with fast T_1, probably indicating a more disordered state but possibly also reflecting the presence of paramagnetic oxygen. However, by annealing the samples at a temperature approximately 5 K below their melting point for a period of order 1 hour, a more ordered material was generally obtained, characterised by a significantly longer spin-lattice relaxation time. The step possibly also enabled some dilution of oxygen in the sample due to the immersion in the helium exchange gas. In practise, aiming to achieve material with very long T_1 was not desirable since it is necessary to practically achieve high levels of ^{1}H polarisation at the beginning of the pulse sequence. Therefore the annealing stage was optimised experimentally to provide material with intermediate values of T_1. Typically, in these experiments the spin-lattice relaxation times were in the range $600 \le T_1 \le 2500$ s at $B = 1$T and $T = 4.2$ K.

4. Results

All NMR spectra in this investigation concern ^{1}H nuclei in the solid state at low temperature.

a) DTP spectroscopy

Using pulse sequence Fig 2a, DTP spectra of thioanisole have been recorded with three low field values B_{lf} = 31.7, 29.7 and 28.8 mT and are presented in Fig. 3. The polarisation field was $B_{pol} = 1$ T and the polarisation time was $\tau_{pol} = 300$ s. The contact between the Zeeman and tunnelling states was conducted at $B_{LC} = 13$ mT for $\tau_{LC} = 2$ s. The NMR resonance field for saturation and measurement of Zeeman polarisation was $B_{nmr} = 0.869$ T, corresponding to a ^{1}H Larmor frequency ν_{nmr} = 37 MHz. The DTP spectra were systematically scanned by incrementing the secondary rf irradiation frequency at each cycle in the sequence in steps of 10 kHz in the range $500 \le \nu_{rf} \le 3600$ kHz with

ACCEPTED MANUSCRIPT

AIP Publishing

This manuscript was accepted by J. Chem. Phys. Click here to see the version of record.

irradiation time $\tau_{lf} = 4$ s. The tunnelling polarisation (vertical axis) is presented as the inverse tunnelling temperature, β_t, recorded after equilibration with the saturated Zeeman reservoir. This polarisation data was calibrated with reference to a measurement of the equilibrium ^{1}H Zeeman polarisation recorded at a field of 100 mT.

Peaks with positive polarity are observed for sideband transitions where $\nu_{rf} = \nu_H - \nu_t$ and $\nu_{rf} = 2\nu_H - \nu_t$, labelled a^- and b^- respectively. Inverted peaks with negative polarity are observed where $\nu_{rf} = \nu_H + \nu_t$ and $\nu_{rf} = 2\nu_H + \nu_t$, labelled a^+ and b^+ respectively. Fitting the peaks in the DTP spectra with Gaussians, we determine the tunnelling frequency, $\nu_t = 560 \pm 3$ kHz.

The peak pair a^+ & a^- are the two members of the $|\Delta m| = 1$ spectrum and are analogous with the DNP features observed in the solid effect [19, 23, 24]. However, whereas in DNP the pair of asymmetric peaks identify forbidden sideband transitions within the manifold of electron-nuclear states, in the DTP experiment recorded here the antisymmetric pair relate to sideband transitions within the manifold of tunnelling-Zeeman states; the role of the electron in DNP has been replaced by the tunnelling CH_3 groups in DTP. The antisymmetric pair of peaks b^+ & b^- have a similar origin, except these are the two members of the $|\Delta m| = 2$ spectrum. Some further insights into these tunnelling polarisation effects will be addressed in Section 5.

In the $B_{lf} = 31.7$ mT spectrum an additional positive peak appears at $\nu_{rf} = 1565$ kHz. We label this b^{2-}, being a sideband peak centred on $\nu_{rf} = 2\nu_H - 2\nu_t$, offset by twice the tunnelling frequency from the centre of the $|\Delta m| = 2$ spectrum. The origin of this peak can only be explained by invoking mechanical coupling between pairs of CH_3 groups [25, 26] and is not accommodated in the simple energy level scheme of Fig. 1a. The simplified energy level scheme for a pair of coupled CH_3 rotors shown in Fig. 1b provides a basis for interpreting these spectral features, where such sidebands may be identified.

Further scrutiny of the spectra as B_{lf} is decreased identifies additional features appearing at ν_H and $2\nu_H$, growing in amplitude as the condition $\nu_H = 2\nu_t$ is approached, where a^+ and b^- begin to overlap. Appearing most clearly in the $B_{lf} = 28.8$ mT spectrum, these NMR peaks are both antisymmetric in shape, reminiscent of the derivative of an absorption peak,. The centres of these 'derivative' shaped peaks accurately identify ν_H and $2\nu_H$ respectively. The NMR linewidth is governed by the ^{1}H-^{1}H

ACCEPTED MANUSCRIPT

AIP Publishing

This manuscript was accepted by J. Chem. Phys. Click here to see the version of record.

dipole interactions, so we infer these antisymmetric features reveal ^{1}H dipolar fine-structure that is not elucidated in the abridged energy level scheme of Fig. 1. In an observation that is possibly related, we also tentatively identify an indication of some antisymmetric structure simultaneously appearing in the a^- and b^+ peaks of the 28.8 mT spectrum. In general the aforementioned peak shapes may indicate the influence of dipolar order, however, these are secondary effects and beyond the scope of the present study.

Acetophenone has a tunnelling frequency[27] that is approximately three times that of thioanisole. DTP spectra have been recorded with $B_{pol} = 1$ T, $B_{LC} = 33$ mT, $\tau_{LC} = 2$ s, $B_{lf} = 39.2$ mT, $\tau_{lf} =$ 5 s and are presented in Fig. 4. Spectra with polarisation times in the range $120 \leq \tau_{pol} \leq 2400$ s are shown. We observe the a^-, a^+ and b^- DTP peaks, however, the frequency of the b^+ peak falls beyond the bandwidth of secondary rf irradiation so could not be accessed with our experimental set up. Analysis of the peak positions provides the tunnelling frequency $\nu_t = 1.428 \pm 0.003$ MHz. Small, inverted features appearing at 1.67 and 3.35 MHz, correspond to the ^{1}H Larmor frequency ν_H and $2\nu_H$ respectively.

DTP spectra of 2-butanone ($\nu_t = 492 \pm 3$ kHz) have been reported earlier [18].

b) Mapping out the level-crossing region, B_{LC}

To investigate the level-crossings between ^{1}H Zeeman and tunnelling CH_3 groups in more detail, the intensity of the DTP spectrum of thioanisole was studied as the level-crossing was approached by varying B_{LC}. In this series of experiments the intensity of the a^- DTP peak was monitored as a function of B_{LC}, thereby mapping out the level-crossing region, see Fig. 5a. With $B_{LC} \geq 30$ mT there is no DTP effect, as the magnetic field is too high to bring the Zeeman and tunnelling systems into contact. As B_{LC} is systematically reduced below 30 mT the DTP signal grows as the tunnelling polarisation is enabled to transfer to the previously saturated Zeeman reservoir in proximity to the level-crossing. Given $\nu_t = 560$ kHz, lc1 will occur where $\nu_H = \nu_t$ at 13.1 mT and lc2 appears at half this field, 6.55 mT. However, in Fig. 5 the DTP effect first appears at twice the field of lc1, namely in the vicinity of 26 mT where $\nu_H = 2\nu_t$. Corroborating the earlier observation, this provides further evidence for mechanical coupling of pairs of CH_3 groups. The level-

ACCEPTED MANUSCRIPT

AIP Publishing

This manuscript was accepted by J. Chem. Phys. Click here to see the version of record.

crossing that facilitates this contact between tunnelling and Zeeman reservoirs, labelled lcc, is shown in the energy level scheme for a pair of coupled CH_3 rotors, Fig. 1b.

Similar behaviour is observed for 2-butanone where the DTP signal peaks at the field B_{LC} =24 mT where $\nu_H = 2\nu_t$, Fig. 5b, so we can infer the coupling of CH_3 pairs may not be uncommon.

In both Figs 5a and 5b, to access the lower field values, it is an unavoidable consequence of the field-cycling sequence that the system first passes through level-crossings that occur at higher field. Therefore, the DTP effect is an integral function of incremental contacts that are made between the two reservoirs as the field switches down to its stable value of B_{LC}. Given plots of DTP signal vs. B_{LC} have a rectangular appearance, as opposed to discrete peaks, we can infer the cross-relaxation process is rapid and highly efficient.

c) The dependence on polarisation time, τ_{pol}

The DTP effect is determined by a polarisation transfer from the ^{1}H Zeeman system to the CH_3 tunnelling system. A population gradient is created within the Zeeman system during the polarisation step. This is subsequently transferred to the tunnelling system by pumping forbidden transitions within the manifold of tunnelling-Zeeman states. To investigate this mechanism quantitatively the intensity of the a^+ and b^- peaks have been measured in thioanisole as a function of τ_{pol}, see Fig. 6a. The DTP signal magnitudes increase systematically with the initial ^{1}H polarisation. Fitting the intensities with a single exponential function we find the two curves grow with time constant 630 ± 30 s which is consistent with the ^{1}H spin-lattice relaxation time at $B_{pol} = 1$ T, confirming the polarisation transfer mechanism.

Similar measurements on 2-butanone and acetophenone are shown in Figs. 6b. In the former the scaled intensity of the DTP signal for the b^- peak is shown superimposed on the growth of the ^{1}H Zeeman polarisation vs. time curve, recorded at $B_{pol} = 1$ T for the same sample. Neither follows a single exponential function but the close superposition of the two sets of data confirms the polarisation transfer mechanism. The behaviour for acetophenone exhibits similar behaviour, but its growth rate reflects the faster average spin-lattice relaxation time of acetophenone at the polarisation field of 1T compared with 2-butanone. Although in none of the experiments conducted on the three samples were the equilibrium conditions quite achieved, it is clear that once the Zeeman system is equilibrated, the DTP effect is maximised under the conditions that pertain.

ACCEPTED MANUSCRIPT

AIP Publishing

This manuscript was accepted by J. Chem. Phys. Click here to see the version of record.

d) The dependence on rf irradiation time, τ_{lf}

The secondary rf irradiation at frequency ν_{rf} drives forbidden transitions among the manifold of tunnelling-Zeeman states. These involve $A \leftrightarrow E$ changes in CH_3 tunnelling state simultaneously with the flip of zero, one or two ^1H spins. These are the tunnelling sideband transitions that give rise to the DTP peaks $a^{\pm}$ and $b^{\pm}$. The efficiency of the irradiation process that pumps these transitions, thereby transferring polarisation from the Zeeman to the tunnelling system, has been investigated by monitoring the DTP peaks as a function of irradiation time, τ_{lf}.

The irradiation time dependence for the a^+ and b^- DTP peaks in thioanisole is shown in Fig. 7a in the range $1 \leq \tau_{lf} \leq 8$ s with $B_{lf} = 29.7$ mT. It is evident $A \leftrightarrow E$ transitions become saturated after approximately 4 s, whereby the connected states have achieved the same population. Therefore the transition rate characterising the process is faster than 1 s^{-1} in this material.

Data for 2-butanone is presented in Fig. 7b. The intensities of a^+, a^-, b^+ and b^- DTP peaks have all been monitored as a function of τ_{lf} at the field $B_{lf} = 27.8$ mT. The growth of the $|\Delta m| = 2$ transitions are both represented well with single exponential functions and transition rates, 0.68 ± 0.07 s^{-1} (b^-) and 0.34 ± 0.06 s^{-1} (b^+). The intensities of the $|\Delta m| = 1$ transitions are already within approximately 80% of the saturated magnitudes after the shortest irradiation time, $\tau_{lf} = 0.5$ s, so precluding accurate measurements of those transition rates. Nevertheless, qualitatively we can conclude the transition rates for $|\Delta m| = 1$ transitions are faster than for $|\Delta m| = 2$ transitions.

Data for the growth of the b^- DTP peak in acetophenone recorded at $B_{lf} = 39.2$ mT is shown in Fig. 7c. Saturation is only approached at times longer than $\tau_{lf} = 20$ s, indicating the transition rate characterising the forbidden sideband transitions in acetophenone is significantly slower than observed for thioanisole and 2-butanone. Fitting with a single exponential, we determine the transition rate governing the forbidden b^- sideband transition to be 0.18 ± 0.03 s^{-1}.

e) Tunnelling lifetime measurements

Applying the protocol depicted in Fig. 2b, where a relaxation step has been introduced into the DTP pulse sequence, the lifetime of the CH_3 tunnelling states has been measured. This is reported in the form of the tunnelling relaxation time and is studied by

ACCEPTED MANUSCRIPT

AIP Publishing

This manuscript was accepted by J. Chem. Phys. Click here to see the version of record.

monitoring the intensity of a DTP peak as a function of magnetic field, B_{rel}. Experiments have been conducted on 2-butanone and thioanisole. For 2-butanone, the intensity of the DTP peak b^- is plotted as a function of relaxation time, τ_{rel}, for several magnetic field values in the range $23.7 \leq B_{rel} \leq 58.7$ mT, see Fig. 8a. Characteristic tunnelling relaxation times, T_{tun}, have been determined by fitting with single exponential decays which generally represent the data well. In Fig. 8b the relaxation data is presented for thioanisole in the range $27.7 \leq B_{rel} \leq 31.7$ mT. Here, particularly at the higher fields, the data appear to be characterised by multi-exponential functions. Nevertheless to facilitate a quantitative analysis of the magnetic field dependence, the data have been fitted with a single exponential decay.

The magnetic field dependence of T_{tun} is plotted in Fig. 8b. Lifetimes at high field, remote from any level-crossings, are relatively long, consistent with the spin-forbidden nature of $A-E$ transitions that require simultaneous changes in spatial and spin quantum states. The fields where $\nu_H = 2\nu_t$ and $\nu_H = \nu_t$ are indicated for both samples, showing how the relaxation time steeply decreases as the level-crossing region is approached. We can infer that in proximity to a level-crossing there is cross-relaxation between Zeeman and tunnelling systems, providing additional pathways, and the tunnelling polarisation is able to relax more efficiently. As earlier, it appears that mechanical coupling between pairs of CH_3 groups means the condition $\nu_H = 2\nu_t$ determines the field where there is efficient contact between the tunnelling and Zeeman systems, rather than lc1.

f) The heat capacity ratio of the Zeeman and tunnelling systems

The DTP pulse sequence involves field-cycling excursions to level-crossings in the tunnelling-Zeeman manifold of levels. This is a practical device to enable the deviations in tunnelling polarisation to be made visible by cross-relaxation between tunnelling and ^{1}H Zeeman reservoirs. The experiments provide limited insight into the detailed cross-relaxation mechanism, but they do reveal this is an efficient process. The extent of thermal mixing between the two reservoirs is determined by their relative heat capacities and experiments have been conducted to investigate this ratio.

We define C_Z and C_t to be the heat capacities of the Zeeman and tunnelling systems respectively. Since the ^{1}H Zeeman splitting is linearly dependent on the applied magnetic field, whereas the tunnelling splitting is independent of field, the heat capacity ratio C_Z/C_t has a different value at the two level-crossings. Following Clough[28] and Zhang[22]

ACCEPTED MANUSCRIPT

AIP Publishing

This manuscript was accepted by J. Chem. Phys. Click here to see the version of record.

statistical thermodynamics provides the respective values, $C_Z/C_t = 3$ at lc1 and $C_Z/C_t = 3/2$ at lc2.

We can devise an experiment to determine C_Z/C_t at a particular field by bringing the two systems into repeated contact. Following the rf irradiation, the [^{1}H Zeeman saturation – τ_{LC} - measurement]$_n$ sequence was repeated n=8 times, at each stage monitoring the intensity of the DTP signal. By such repetitions, the tunnelling polarisation is diluted at each stage of contact with the saturated Zeeman system and we expect the DTP intensity to follow a geometric decline, enabling an estimate of C_Z/C_t to be made. Such an experiment has been conducted on 2-butanone, where the amplitude of the b^- DTP peak is plotted vs. the number of level-crossing contacts, n, Fig. 9. The data is presented as the ratio of the DTP signal after the n'th contact relative to the first, (P_n/P_1). For this experiment the level-crossing contact was made at the field B_{LC} = 12 mT, representing lc1. If the initial inverse temperatures are β_Z and β_t then when contact is made the two systems come to the common inverse temperature $\left(\frac{C_Z}{C_t}\beta_Z + \beta_t\right) \Big/ \left(\frac{C_Z}{C_t} + 1\right)$. However, at each cycle the Zeeman system is saturated, so the decline of the DTP signal conforms with the function $(P_n/P_1) = \left(\frac{C_Z}{C_t} + 1\right)^{-n}$. Already by the second contact the DTP signal has declined to 16% of its value at the first contact, P_1. By the third contact it is smaller than experimental uncertainties. In these circumstances we cannot extract an accurate value of the heat capacity ratio, but by fitting with the function $(C_Z/C_t + 1)^{-n}$, the data in Fig. 9 do permit upper and lower limits to be placed on the heat capacity ratio. We find, $5 < C_Z/C_t < 8$.

5. Discussion and numerical simulations

The field-cycling sequence has been shown to successfully manipulate the tunnelling polarisations. Changes in tunnelling state can be driven in a prescribed manner by rf irradiation, pumping selective tunnelling sideband transitions. Additionally, as part of this sequence, the contact between the two systems established at a level-crossing enables the tunnelling state to be interrogated via a measurement of the ^{1}H Zeeman magnetisation. Tunnelling polarisations are achieved with magnitudes that are comparable with the equilibrium ^{1}H Zeeman polarisations. The mechanisms involved are

ACCEPTED MANUSCRIPT

AIP Publishing

This manuscript was accepted by J. Chem. Phys. Click here to see the version of record.

analogous to DNP and the solid effect, except the role of the electron in DNP is replaced by the CH_3 tunnelling system in DTP.

By selecting the appropriate tunnelling sideband, both positive and negative tunnelling polarisations are achieved. So the tunnelling system may be cooled, or alternatively heated to the extent that a population inversion can be induced. This facility enhances the degree to which the tunnelling system can be manipulated in a prescribed manner.

To gain further insight into the mechanisms, a thermodynamic model has been developed which provides the theoretical basis for a simulation of the DTP spectrum. This model is a development of earlier publications by the Nottingham group, to which the reader is referred for further details [22, 28-30]. Forming the basis of the simulation, for a given applied magnetic field and tunnelling frequency the matrix of the spin Hamiltonian $\hat{H}_s$, Eqn. (1), may be written directly in the basis of spin functions $\left|m_{I1}m_{I2}m_{I3}\right\rangle$, or alternatively in symmetry-adapted form[10,22]. Then following ref. [22], the eigenvalues and eigenfunctions of the CH_3 system are calculated by numerical diagonalization of $\hat{H}_s$. This determines the extent to which there is a mixing of the A and E states by the non-secular terms in the dipolar interaction. The thermodynamic parameters, namely the populations, polarisations and inverse temperatures of the ^{1}H Zeeman and tunnelling systems are defined according to the framework described in section 2, Eqns. (4) – (6). Then those thermodynamic parameters are evolved in a step-wise fashion imitating each stage of the field-cycling pulse sequence, Fig. 2a. Here, to simulate the effects of rf irradiation at low field, the changes in population of states labelled i and j that participate in a weakly allowed tunnelling sideband transition may be written as [22],

$$\begin{aligned}\frac{dp_i}{dt} &= T_{i\leftrightarrow j}\left(p_i - p_j\right)\\ \frac{dp_j}{dt} &= T_{j\leftrightarrow i}\left(p_j - p_i\right)\end{aligned} \qquad (7)$$

where using the eigenvectors calculated from the diagonalization of $\hat{H}_s$, the transition rates per unit time, $T_{i\leftrightarrow j}$, are determined by Fermi's golden rule with the time-dependent Zeeman Hamiltonian $\hat{H}_{rf} = \hbar\gamma B_1\hat{I}_x$. Here B_1 is the amplitude of the rf field.

Evolution also occurs in response to the switches in magnetic field between B_{z1} and B_{z2} that arise in the field-cycling sequence. These are adiabatic, resulting in adiabatic magnetisation/demagnetisation of the system depending on the direction of the field switch. Accordingly the change in inverse ^{1}H Zeeman temperature that accompanies a field switch is calculated using,

ACCEPTED MANUSCRIPT

AIP Publishing

This manuscript was accepted by J. Chem. Phys. Click here to see the version of record.

$$\beta_{Z2} = \frac{B_{z1}}{B_{z2}} \beta_{Z1} \tag{8}$$

Additionally, at a level-crossing the cross-relaxation between the respective systems induces changes in inverse temperature of the two systems described by the pair of differential equations [22],

$$\begin{aligned} \frac{d\beta_Z}{dt} &= W\left(\beta_Z - \beta_t\right)\frac{C_t}{C_t + C_Z} \\ \frac{d\beta_t}{dt} &= W\left(\beta_t - \beta_Z\right)\frac{C_Z}{C_t + C_Z} \end{aligned} \tag{9}$$

where W is the cross-relaxation rate.

Therefore, the solutions of $\hat{H}_s$ provide the eigenvalues and eigenfunctions, Eqns. (4) – (6) define the thermodynamic parameters and Eqns. (7) – (9) are used to evolve them. At each step in the pulse sequence this involves a simulation of the populations of the eigenstates. The model has been applied to simulate the DTP spectra of thioanisole with $\nu_t = 560$ kHz. The dipolar terms in the matrix of $\hat{H}_s$ are calculated assuming the CH_3 rotor adopts a tetrahedral configuration with hydrogen atoms forming a rigid equilateral triangle with C-H bond length 1Å. The transition probabilities are calculated using the eigenvectors and a powder average determined from which the overall transition rates for each sideband may be evaluated.

Many of the parameters in the simulation are determined by the experimental conditions or defined by the terms in the spin Hamiltonian indicated earlier. The initial ^{1}H Zeeman polarisation is estimated given the known value of T_1 at the polarisation field and the polarisation time. For direct comparison with experiment, the baselines of the DTP spectra reflect the initial tunnelling polarisation so the corresponding inverse temperatures used in the simulations are $\beta_t^{(init)} = 0.260 \pm 0.005\,\mathrm{K}^{-1}$, $0.224 \pm 0.005\,\mathrm{K}^{-1}$, and $0.194 \pm 0.005\,\mathrm{K}^{-1}$ respectively for magnetic fields of 28.8 mT, 29.7 mT and 3.17 mT, see Fig. 3. The cross-relaxation rate at the level-crossings was simulated by a Gaussian function, $W(B) = W_0 \exp\left(-\left(B - B_{LC}\right)/\sigma^2\right)$ with $W_0 = 10$ s^{-1} and $\sigma = 3$ mT. The Gaussian width parameter σ was estimated from the solutions of $\hat{H}_s$, plotting the energy levels vs. applied magnetic field. The amplitude of the rf field of the secondary irradiation channel, $B_1 = 0.95$ mT, was estimated from the coil geometry and its electrical characteristics in combination with the rf power amplifier. Using this value of B_1 the

ACCEPTED MANUSCRIPT

AIP Publishing

This manuscript was accepted by J. Chem. Phys. Click here to see the version of record.

transition probabilities calculated from $\hat{H}_s$ and employed in the simulations are given in Table 1.

The simulated DTP spectra for thioanisole are presented in Fig. 3 with solid lines. There is generally good quantitative agreement with experiment for the features associated with sidebands a^+, a^-, b^+ and b^-, confirming the proposed mechanisms that form the basis of the thermodynamic model. The model does not address mechanical coupling so the double sideband feature $2b^-$ does not appear in the simulation. Neither in the simulation do the 'derivative' lineshape features appear at ν_H or $2\nu_H$ when the condition $\nu_H = 2\nu_t$ is approached, since the dipolar order is not considered.

The transition rates for thioanisole calculated from the Hamiltonian (Table 1) are of order, $T \approx 0.3\,\mathrm{s}^{-1}$. This is qualitatively consistent with the growth of the DTP peaks as a function of irradiation time, τ_{lf}, shown in Fig. 7a, providing further validation for the simulated DTP spectra. Since thioanisole and 2-butanone have similar tunnelling frequencies and therefore similar $\hat{H}_s$, a more quantitative comparison is available from the data for 2-butanone, Fig. 7b and the calculated transition rates for thioanisole in Table 1. Experimental and theoretical values for the $|\Delta m| = 2$ sidebands agree within a factor two and the transition rates for the $|\Delta m| = 1$ sidebands are systematically faster in both experimental and calculated data sets. This represents a favourable comparison given the uncertainties in modelled and experimental parameters, for example B_1.

It is pertinent to address here in further detail the mechanisms driving the tunnelling sidebands and which give rise to the prescribed manipulations of the tunnelling polarisation. In conventional DNP, 'forbidden' transitions among the manifold of electron -nuclear spin states are rendered weakly allowed by non-secular terms in the electron-nuclear interaction which mix the pure basis states. The transitions in question involve simultaneous changes in electron spin and nuclear spin states. As described by Abragam[31], pumping such forbidden transitions which occur in proximity to the electron spin resonance frequency, ν_e, gives rise to strong positive and negative deviations in nuclear spin polarisation, depending on the sign of the offset, $\nu_e \pm \nu_n$, forming the basis of the solid effect. In the DTP experiment with CH_3 quantum rotors, we identify 'forbidden' transitions among the manifold of tunnelling-Zeeman states. These involve A $\leftrightarrow$ E changes in nuclear spin-symmetry, representing simultaneous changes in tunnelling and nuclear spin states. These are the methyl tunnelling sidebands in NMR, offset from

ACCEPTED MANUSCRIPT

AIP Publishing

This manuscript was accepted by J. Chem. Phys. Click here to see the version of record.

the nuclear spin resonance frequency by $\pm\nu_t$. These 'forbidden' transitions are rendered weakly allowed due to mixing of A and E states by the non-secular terms in the ^{1}H-^{1}H dipole-dipole interaction. Pumping these forbidden transitions drives the strong positive and negative deviations in tunnelling polarisation, depending on the sign of the offset. The non-secular terms in $\hat{H}_{dd}$ involve single spin-flip operators such as $\hat{I}_z\hat{I}_+$ which are responsible for $|\Delta m|=1$ sideband transitions, but additionally there are double spin-flip operators such as $\hat{I}_+\hat{I}_+$ which facilitate $|\Delta m|=2$ sidebands. The $|\Delta m|=1,2$ tunnelling sidebands are strongly forbidden at conventional magnetic fields employed in NMR, but as the dipolar energies become more comparable to the nuclear Zeeman energy at low field, both single and double spin-flip components become more strongly allowed. Therefore, analogous to DNP and the solid effect, the DTP spectrum comprises positive and negative peaks in tunnelling polarisation symmetrically displaced about the nuclear spin resonance frequency. However, because of the double spin-flip operators, a $|\Delta m|=2$ spectrum is also observed, mirroring that of $|\Delta m|=1$.

The field-cycling methods facilitate field-dependence measurements of the tunnelling relaxation time, Fig. 8. With field offsets of just 5 or 10 mT from a level-crossing, values of T_{tun} are already very long, confirming the ^{1}H Zeeman and tunnelling systems are normally strongly decoupled at low temperatures. However, there is a steep decrease in T_{tun} as the level-crossings are approached and cross-relaxation pathways become efficient. The field-offsets in question, of order 5 or 10 mT, are noteworthy, being of the order of the NMR linewidths. The latter are governed by ^{1}H-^{1}H dipolar interactions, so given $\hat{H}_{dd}$ contains the requisite space-spin coupled terms that can drive transitions between A and E states, we find confirmatory evidence for the important role that the dipolar Hamiltonian plays in tunnelling relaxation specifically and quantum rotor physics more generally. Although the field-switching timescales do not enable a closer approach to the level-crossing in these tunnelling relaxation experiments, the study does probe the same cross-relaxation process that is responsible for bringing the tunnelling and Zeeman reservoirs into contact at a level-crossing. Extrapolating the curve of T_{tun} vs. B_{rel} in Fig. 8c, the data seems consistent with the cross-relaxation rate value $W_0=10$ s^{-1} employed in the simulations.

The experiments in section 4f reveal the heat capacity ratio is somewhat larger than the value $C_Z/C_t=3$ derived from a statistical analysis of the manifold of tunnelling-Zeeman energy levels[22, 28]. Firstly it should be noted there are additional non-methyl protons

ACCEPTED MANUSCRIPT

AIP Publishing

This manuscript was accepted by J. Chem. Phys. Click here to see the version of record.

present in the molecule which, as a result of efficient spin diffusion processes, contribute to the heat capacity of the ^{1}H Zeeman reservoir. Secondly, the theoretical value 3 is only valid for isolated groups at the field corresponding to lc1. However mechanical coupling means the manifold of coupled rotor states is more complex than provided for in a statistical thermodynamic analysis of the energy levels of Fig. 1a. Moreover the field-cycling switches that characterise the pulse sequence transit through the level crossing lcc which occurs at higher field than lc1. Therefore, the situation is complex but taking all these factors into account it is to be expected the experimental value $5 < C_Z/C_t < 8$ deviates from the theoretical value 3.

A series of experiments were conducted on acetophenone as a function of time spent at the level-crossing, τ_{LC}. Allowing for the duration of a field-switch, in these experiments the shortest practicable time was approximately 0.1 s. However, in the range $0.1 \leq \tau_{LC} \leq 2$ s, no significant dependence of the DTP signal on contact time between Zeeman and tunnelling systems was noted, indicating that the polarisation transfer occurs on a timescale faster than 100 ms. Similar behaviour was noted for 2-butanone and thioanisole. Experimentally the system traverses the outlying parts of the level-crossing region during the field switch to the level-crossing field, B_{LC}. Therefore, such experiments are unable to quantitatively investigate the dependence on τ_{LC} precluding any accurate measure of the cross-polarisation rate, W in that way. Nevertheless, these observations make it clear that cross-relaxation is fast at the level-crossings and the value employed in the simulations for thioanisole, $W_0 = 10\ \mathrm{s}^{-1}$ is consistent with experiment.

6. Concluding remarks

These investigations were devised to develop techniques that enable the polarisation of a methyl tunnelling system to be probed and manipulated in a prescribed fashion. Using magnetic field-cycling NMR pulse sequences and irradiating forbidden transitions within the manifold of ^{1}H tunnelling-Zeeman energy levels, this has been achieved. It has proved possible to invert the tunnelling populations as well as create tunnelling states characterised by relatively low temperatures. The mechanisms are analogous to DNP and the solid effect. Comparing with those established techniques, the role of the electron spin in DNP is replaced by the tunnelling methyl system in these DTP phenomena. The effect relies on a polarisation transfer between ^{1}H Zeeman and tunnelling systems mediated by rf irradiation at the various tunnelling sidebands. Therefore, the tunnelling polarisations achievable are consistent with those characterising a nuclear spin system. The experiments provide insights into the physics of space-spin entangled systems such

ACCEPTED MANUSCRIPT

AIP Publishing

This manuscript was accepted by J. Chem. Phys. Click here to see the version of record.

as those which typify quantum rotors. This is interesting to broader studies seeking to employ quantum rotors in nuclear spin polarisation schemes. Informed by parameters determined from the eigenstates of the system's Hamiltonian, a simple thermodynamic model has been described which provides quantitative agreement with experiment. One finding that reveals itself repeatedly in different ways is that mechanical coupling between pairs of methyl groups is surprisingly prevalent. This means the simple model of an isolated methyl group, while generally adequate to account for many methyl-related phenomena, requires improvement to account for the full range of observations.

Acknowledgment

S.M.M.A.K is grateful to the Iraq Ministry of Higher Education and Scientific Research for the award of a postgraduate scholarship.

ACCEPTED MANUSCRIPT

AIP Publishing

This manuscript was accepted by J. Chem. Phys. Click here to see the version of record.

Table 1. Calculated tunnelling sideband transition rates for thioanisole ($\nu_t = 560$ kHz) used in the simulated DTP spectra of Fig. 3. The rf field amplitude is $B_1 = 0.95$ mT.

T^{a^+}	T^{a^-}	T^{b^+}	T^{b^-}
0.34 s^{-1}	0.39 s^{-1}	0.17 s^{-1}	0.22 s^{-1}

ACCEPTED MANUSCRIPT

AIP Publishing

This manuscript was accepted by J. Chem. Phys. Click here to see the version of record.

Figure Legends

Fig. 1 The manifold of tunnelling-Zeeman energy levels, showing the level-crossings lc1, lc2 and lcc (see main text for details): a) single CH_3 group, indicating tunnelling sideband transitions; b) mechanically coupled pairs of CH_3 groups (simplified with $\hat{H}_{dd}$ omitted). The arrows denote the forbidden transitions connecting A and E states that are responsible for the respective tunnelling sideband peaks in the DTP spectra.

Fig. 2 The field-cycling NMR pulse sequences employed in the DTP experiments: a) DTP pulse sequence, b) DTP pulse sequence including a tunnelling relaxation step.

Fig. 3 DTP spectra of thioanisole ($\nu_t = 560 \pm 3$ kHz) recorded at three applied magnetic fields, B_{lf} = 28.8, 29.7 and 31.7 mT. Other pulse sequence parameters: $\tau_{lf} = 4$ s, B_{pol} = 1 T, $\tau_{pol} = 300$ s, $B_{LC} = 13$ mT, $\tau_{LC} = 2$ s, T = 4.2 K. The polarisation pertaining to the tunnelling reservoir immediately after the level-crossing induced cross-relaxation with the saturated ^{1}H system is represented as an inverse temperature, β_t. The solid lines represent the simulations discussed in section 5.

Fig. 4 DTP spectra of acetophenone recorded at $B_{lf} = 39.2$ mT, $\nu_t = 1.428 \pm 0.003$ MHz. Other pulse sequence parameters: $\tau_{lf} = 5$ s, $B_{pol} = 1$ T, $B_{LC} = 33$ mT, $\tau_{LC} = 2$ s, T = 4.2 K. With emphasis on the b^- peak, the spectra have been recorded as a function of polarisation time, τ_{pol}.

Fig. 5 The DTP peak intensity (b^-) as a function of B_{LC}, mapping out the contact between the Zeeman and tunnelling states in the level crossing region; a) thioanisole, b) 2-butanone.

Fig. 6 The DTP peak intensity as a function of polarisation time, τ_{pol}: a) thioanisole, a^+ and b^- peaks; b) b^- peak intensities for acetophenone (filled squares) and 2-butanone (filled circles), superimposing the polarisation growth vs. time curve for 2-butanone recorded at the same field, $B_{pol} = 1$ T (open squares).

Fig. 7 The DTP peak intensity as a function of irradiation time, τ_{lf}: a) thioanisole, a^+ and b^- peaks plotted as $f(\nu_{rf})$; b) 2-butanone, a^+, a^-, b^+ and b^- peak intensities; c) acetophenone, b^- peak intensity.

ACCEPTED MANUSCRIPT

AIP Publishing

This manuscript was accepted by J. Chem. Phys. Click here to see the version of record.

Fig. 8 The relaxation of the tunnelling reservoir recorded for several relaxation fields, B_{rel} : a) relaxation curves for 2-butanone; b) relaxation curves for thioanisole; c) tunnelling relaxation times, T_{tun} , as a function of B_{rel} .

Fig. 9 Determining the heat capacity ratio, C_Z/C_t in 2-butanone by monitoring the b- peak intensity while making repeated contacts between ^{1}H Zeeman and tunnelling reservoirs. The solid line is the function $\left(P_n/P_1\right)=\left(C_Z/C_t+1\right)^{-n}$ with C_Z/C_t = 6.5.

ACCEPTED MANUSCRIPT

AIP Publishing

This manuscript was accepted by J. Chem. Phys. Click here to see the version of record.

References

1 A. J. Horsewill, et al., Physical Review B **85**, 205440 (2012).
2 M. Carravetta, et al., Physical Chemistry Chemical Physics **9**, 4879 (2007).
3 S. Mamone, J. Y. C. Chen, R. Bhattacharyya, M. H. Levitt, R. G. Lawler, A. J. Horsewill, T. Room, Z. Bacic, and N. J. Turro, Coordination Chemistry Reviews **255**, 938 (2011).
4 M. Carravetta, O. G. Johannessen, and M. H. Levitt, Physical Review Letters **92** (2004).
5 B. Meier, et al., Journal of the American Chemical Society **135**, 18746 (2013).
6 M. Carravetta and M. H. Levitt, Journal of the American Chemical Society **126**, 6228 (2004).
7 W. Press, *Single-Particle Rotations in Molecular Crystals* (Springer-Verlag, Berlin Heidelberg New York, 1981).
8 A. J. Horsewill, Progress in Nuclear Magnetic Resonance Spectroscopy **35**, 359 (1999).
9 J. H. Freed, Journal of Chemical Physics **43**, 1710 (1965).
10 F. Apaydin and S. Clough, Journal of Physics Part C Solid State Physics **1**, 932 (1968).
11 R. A. Green, R. W. Adams, S. B. Duckett, R. E. Mewis, D. C. Williamson, and G. G. R. Green, Progress in Nuclear Magnetic Resonance Spectroscopy **67**, 1 (2012).
12 M. Tomaselli, C. Degen, and B. H. Meier, Journal of Chemical Physics **118**, 8559 (2003).
13 M. Tomaselli, U. Meier, and B. H. Meier, Journal of Chemical Physics **120**, 4051 (2004).
14 S. S. Roy, J.-N. Dumez, G. Stevanato, B. Meier, J. T. Hill-Cousins, R. C. D. Brown, G. Pileio, and M. H. Levitt, Journal of Magnetic Resonance **250**, 25 (2015).
15 J. N. Dumez, et al., Journal of Chemical Physics **142** (2015).
16 M. Icker and S. Berger, Journal of Magnetic Resonance **219**, 1 (2012).
17 M. Icker, P. Fricke, and S. Berger, Journal of Magnetic Resonance **223**, 148 (2012).
18 A. J. Horsewill and S. M. M. Abu-Khumra, Physical Review Letters **107** (2011).
19 A. Abragam and W. G. Proctor, Comptes Rendus Hebdomadaires Des Seances De L Academie Des Sciences **246**, 2253 (1958).
20 A. Abragam, *The Principles of Nuclear Magnetism* (Clarendon Press, Oxford, 1961).
21 M. Prager and A. Heidemann, Chem. Rev. **97**, 2933 (1997).
22 B. Zhang and A. J. Horsewill, Journal of Magnetic Resonance **258**, 33 (2015).
23 C. D. Jeffries, Physical Review **117**, 1056 (1960).
24 K. R. Thurber and R. Tycko, Journal of Chemical Physics **137** (2012).
25 S. Clough, A. Heidemann, A. H. Horsewill, and M. N. J. Paley, Zeitschrift Fur Physik B-Condensed Matter **55**, 1 (1984).
26 S. Clough and Z. T. Lalowicz, Journal of Physics C-Solid State Physics **6**, L452 (1973).
27 A. M. Alsanoosi, A. J. Horsewill, and S. Clough, Journal of Physics-Condensed Matter **1**, 643 (1989).
28 S. Clough, A. J. Horsewill, and P. J. McDonald, Journal of Physics C-Solid State Physics **17**, 1115 (1984).
29 M. J. Barlow, S. Clough, P. A. Debenham, and A. J. Horsewill, Journal of Physics-Condensed Matter **4**, 4165 (1992).
30 A. J. Horsewill and C. Sun, Journal of Magnetic Resonance **199**, 10 (2009).
31 A. Abragam and M. Goldman, Rep. Prog. Phys. **41**, 395 (1978).

ACCEPTED MANUSCRIPT

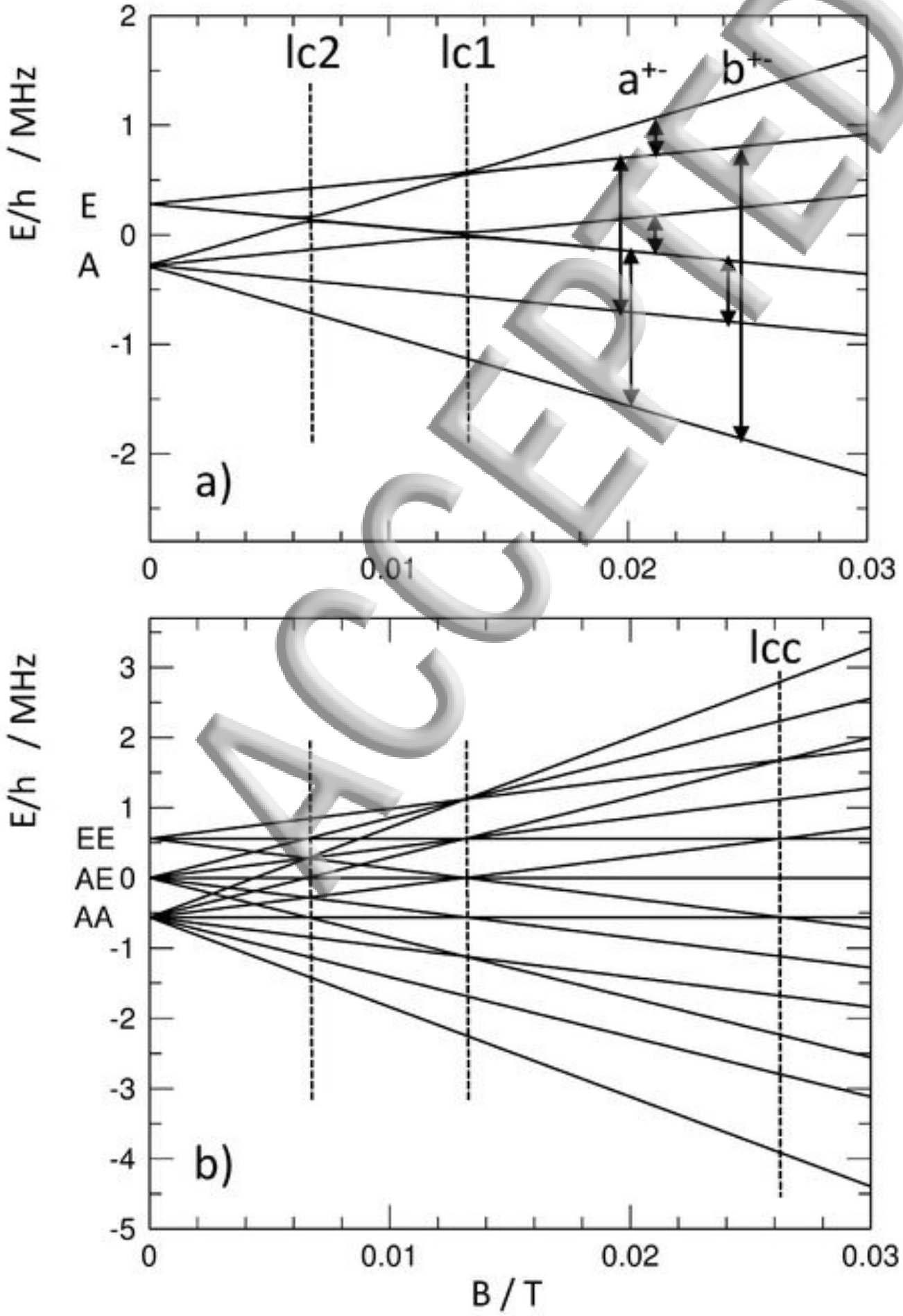

ACCEPTED

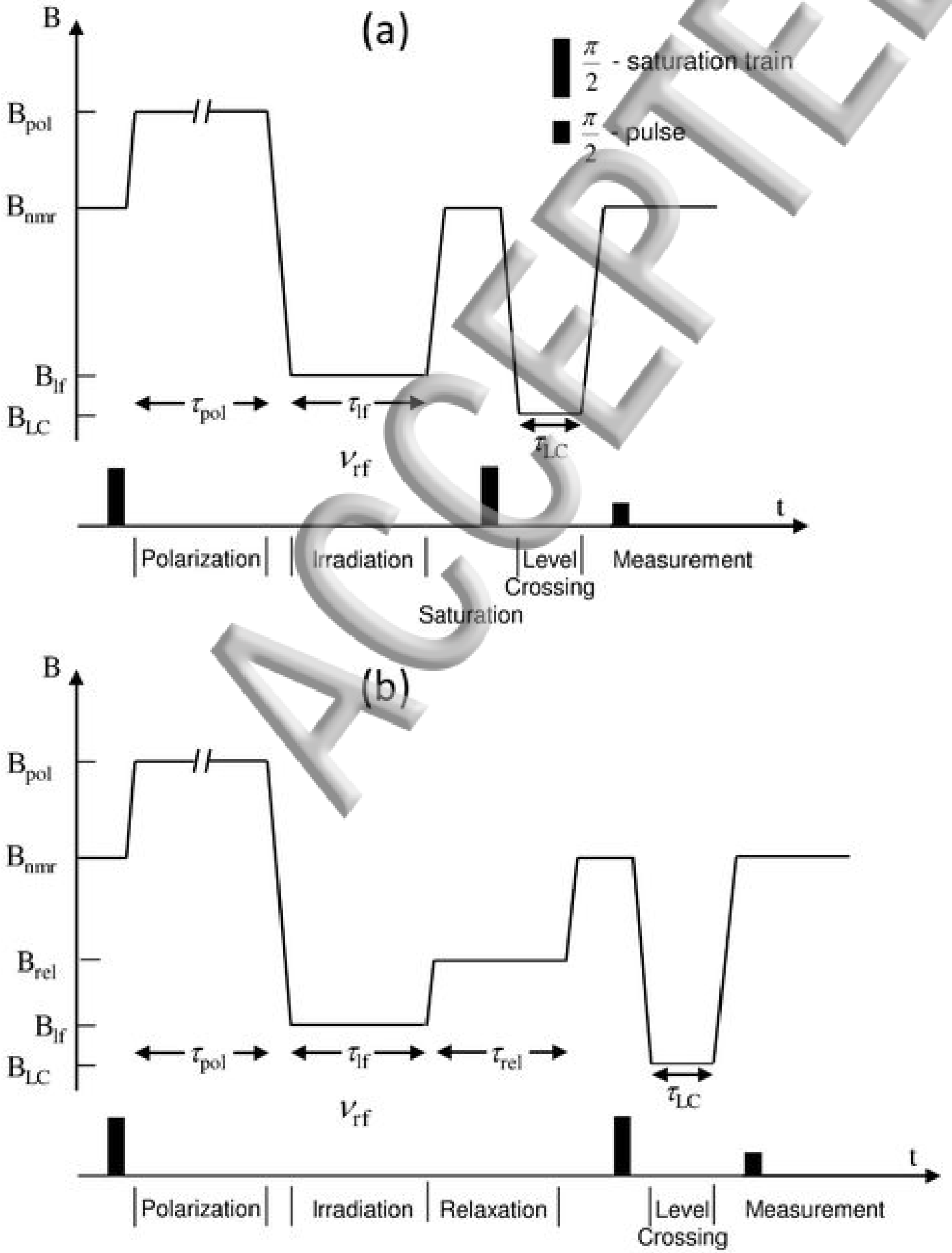
(a)
B
B_{pol}
B_{nmr}
B_{lf}
B_{LC}
$\frac{\pi}{2}$ - saturation train
$\frac{\pi}{2}$ - pulse
τ_{pol}
τ_{lf}
τ_{LC}
ν_{rf}
t
Polarization
Irradiation
Level Crossing
Saturation
Measurement
(b)
B
B_{pol}
B_{nmr}
B_{rel}
B_{lf}
B_{LC}
τ_{pol}
τ_{lf}
τ_{rel}
τ_{LC}
ν_{rf}
t
Polarization
Irradiation
Relaxation
Level Crossing
Measurement

ACCEPTED

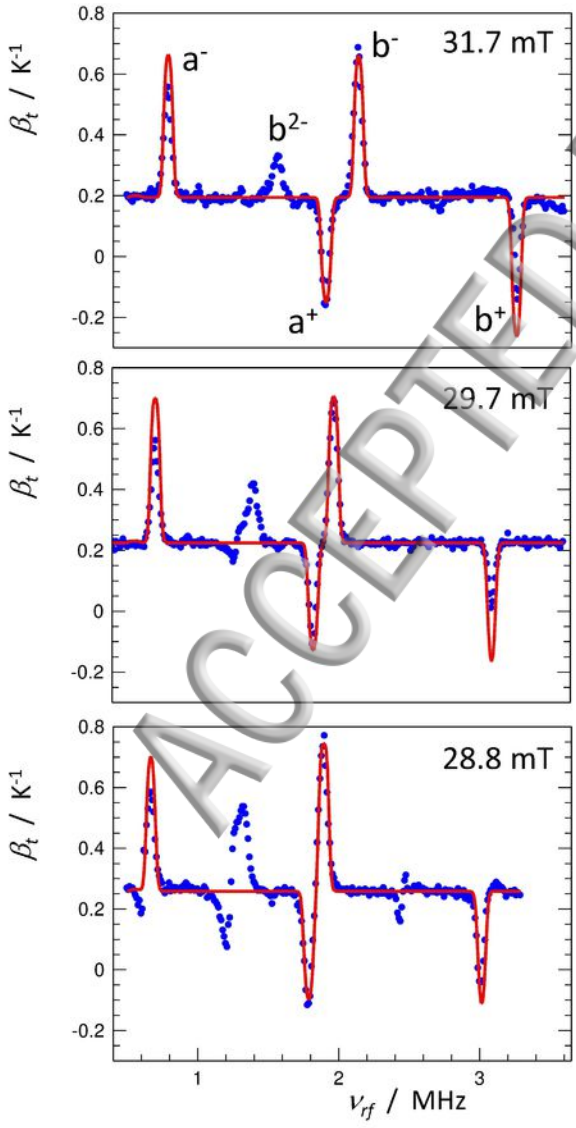

ACCEPTED

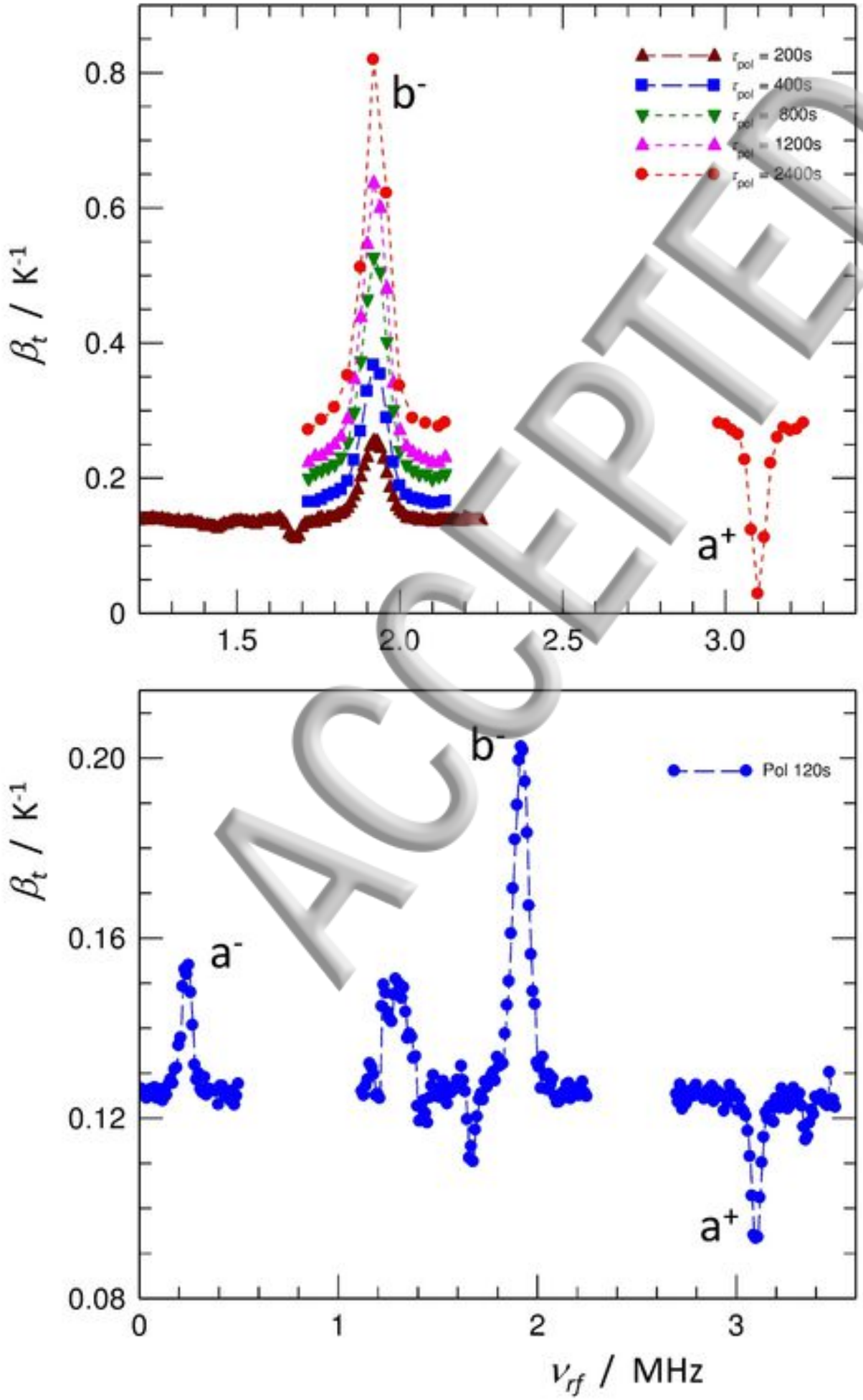
0.8
0.6
0.4
0.2
0
β_t / K^{-1}
b$^-$
τ_{pol} = 200s
τ_{pol} = 400s
τ_{pol} = 800s
τ_{pol} = 1200s
τ_{pol} = 2400s
a$^+$
1.5
2.0
2.5
3.0
0.20
0.16
0.12
0.08
β_t / K^{-1}
b$^-$
Pol 120s
a$^-$
a$^+$
0
1
2
3
ν_{rf} / MHz

ACCEPTED

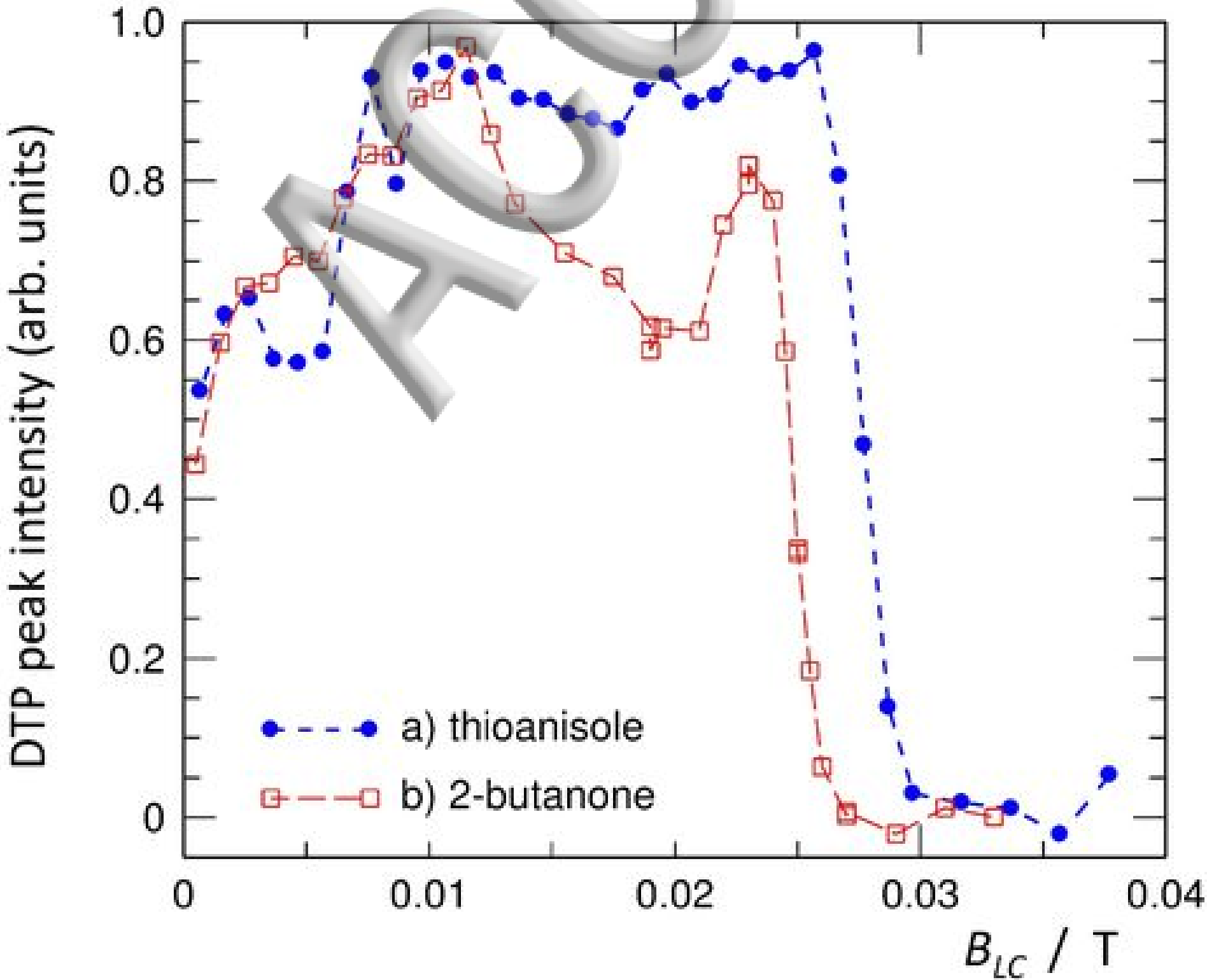
DTP peak intensity (arb. units)
1.0
0.8
0.6
0.4
0.2
0
0
0.01
0.02
0.03
0.04
B_{LC} / T
a) thioanisole
b) 2-butanone

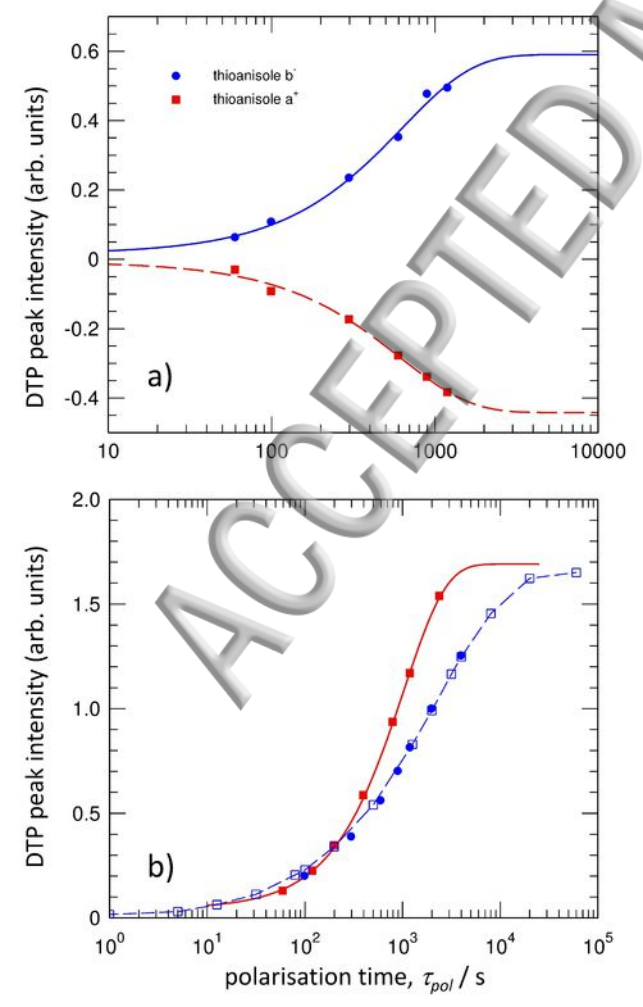
thioanisole b⁻
thioanisole a⁺
DTP peak intensity (arb. units)
a)
b)
polarisation time, τ_{pol} / s

ACCEPTED

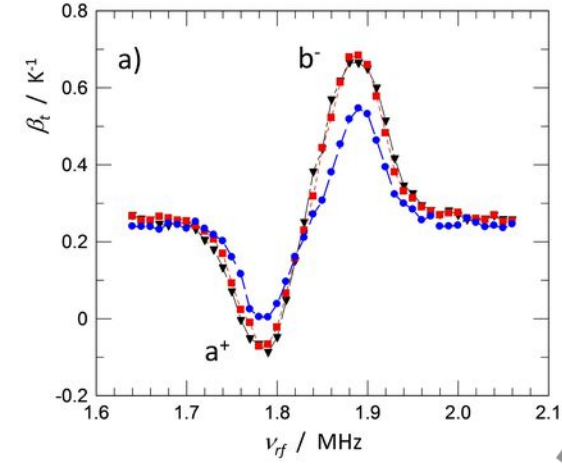
a)
b⁻
a⁺
β_t / K^{-1}
ν_{rf} / MHz

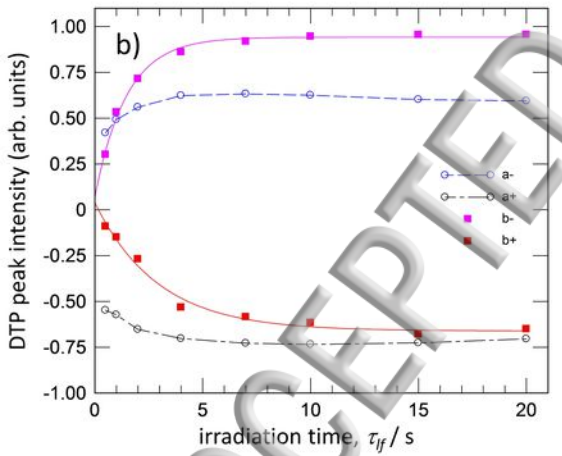
b)
a-
a+
b-
b+
DTP peak intensity (arb. units)
irradiation time, τ_{lf} / s

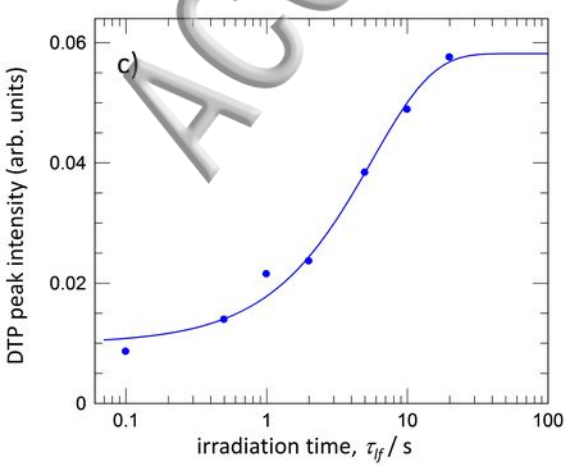
c)
DTP peak intensity (arb. units)
irradiation time, τ_{lf} / s

ACCEPTED

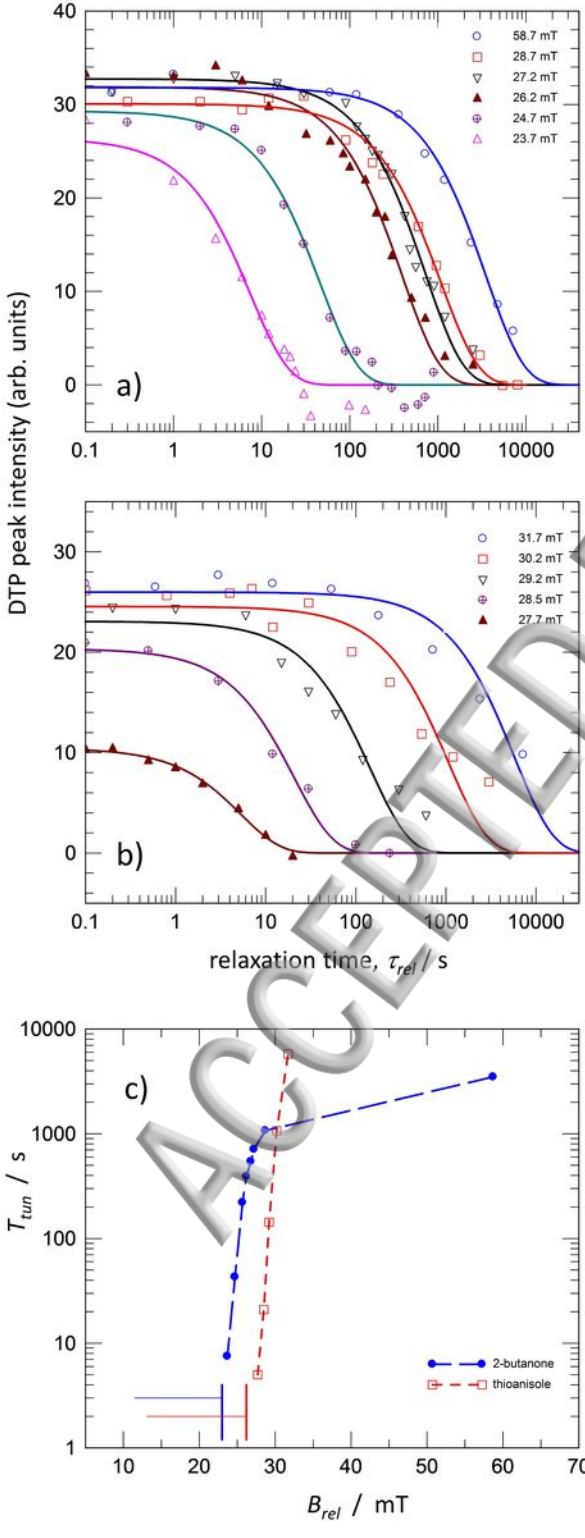
a)
58.7 mT
28.7 mT
27.2 mT
26.2 mT
24.7 mT
23.7 mT
b)
31.7 mT
30.2 mT
29.2 mT
28.5 mT
27.7 mT
DTP peak intensity (arb. units)
relaxation time, τ_{rel} / s
c)
T_{tun} / s
B_{rel} / mT
2-butanone
thioanisole

ACCEPTED

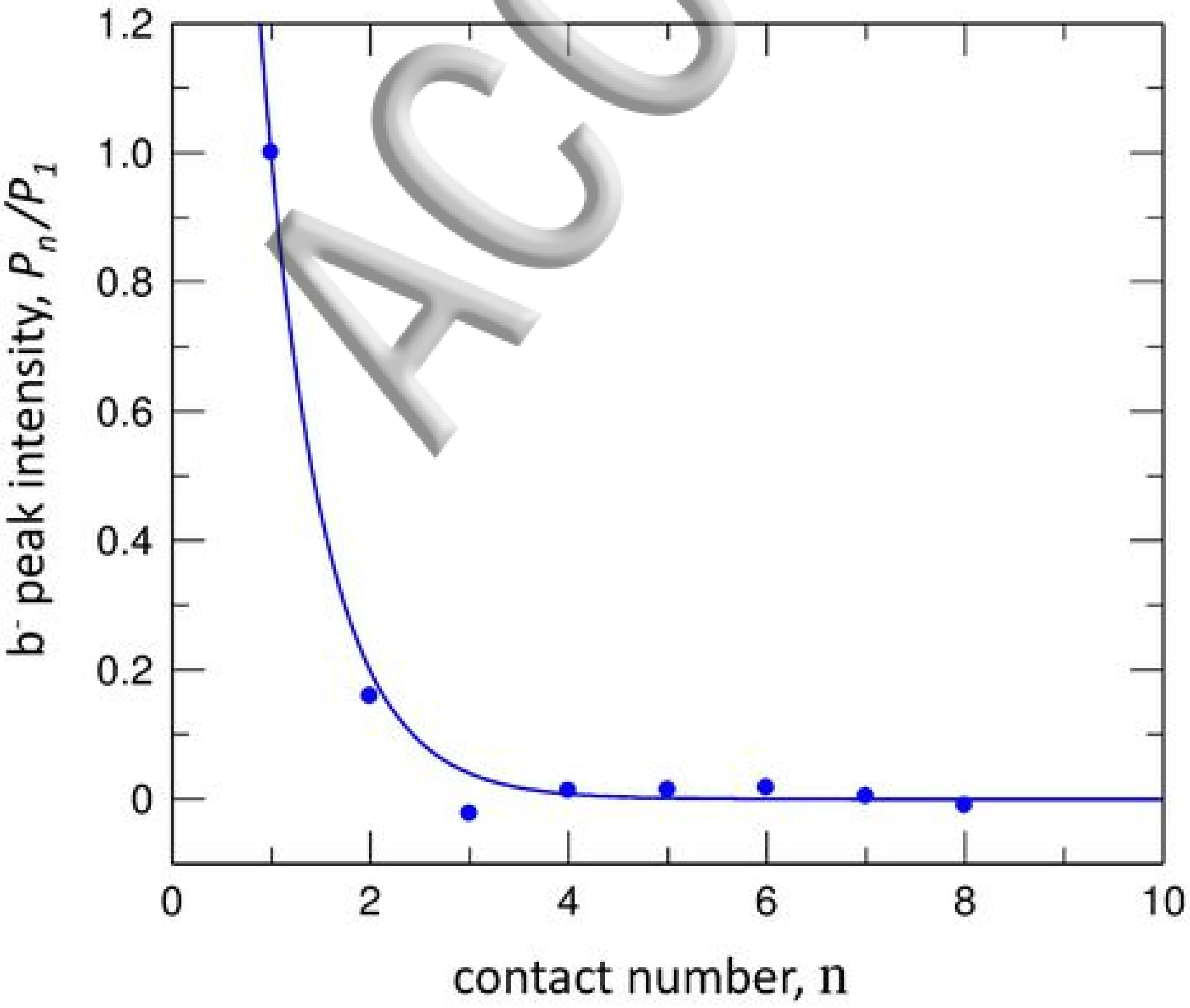
1.2
1.0
0.8
0.6
0.4
0.2
0
b⁻ peak intensity, P_n/P_1
0
2
4
6
8
10
contact number, n